Vol 3 (1) (2022)

Measurement, Control, and Automation

Website: https:// mca-journal.org

ISSN 1859-0551

Anti-sway and position control for double-pendulum crane using IS-ADRC controller

Tan Minh Nguyen, Minh Duc Duong, Trong Hieu Do

Hanoi University of Science and Technology
Corresponding authors E-mail: duc.duongminh@hust.edu.vn, hieu.dotrong@hust.edu.vn

Abstract

Gantry cranes are widely used in various fields such as industry and transportation. However, the crane generates unwanted payload vibration during operation, causing operation and safety at work difficulties. Especially with double-pendulum cranes, this is even more serious. This paper proposed the ADRC and Input Shaping combination controller to control trolley position and suppress payload vibration. The Equal Shaping-Time and Magnitude (ETMn) is presented and compared to the traditional Input Shaping method. Simulation results show the effectiveness of the proposed method.

***Keywords**: ADRC; Input Shaping; Double-Pendulum Crane; Impulse Vector; Vibration Suppression*

Symbols

Symbols	Units	Description
A, **B**, **C**, **L**		state-space matrix
$G(s)$		transfer function
ω_n, ω_d	rad/s	natural frequency
ζ		damping ratio
θ_1, θ_2	rad	sway angle
x	m	trolley position

Abbreviations

ADRC	Active Disturbance Rejection Control
IS	Input Shaping
ZV	Zero Variation
ZVD	Zero Variation & Derivative
ZVDD	Zero Variation Derivative & Derivative
ETMn	Equal Shaping-Time and Magnitude

Tóm tắt

Cầu trục được sử dụng rộng rãi trong nhiều lĩnh vực khác nhau như công nghiệp và giao thông vận tải. Tuy nhiên, trong quá trình hoạt động, cầu trục phát sinh rung động không mong muốn của tải trọng, gây khó khăn trong vận hành và an toàn khi làm việc. Đặc biệt với cầu trục con lắc đôi thì điều này càng khó khăn hơn. Bài báo này đã đề xuất bộ điều khiển kết hợp ADRC và Input Shaping trong việc điều khiển vị trí của tải trọng và hạn chế rung động của tải trọng. Phương pháp tạo dạng với thời gian định hình và biên độ bằng nhau (ETMn) được trình bày để so sánh với phương pháp tạo dạng đầu vào truyền thống. Các kết quả mô phỏng cho thấy hiệu quả của phương pháp đề xuất.

1. Introduction

There are many control methods to suppress vibration and control the crane position in recent years, especially for double pendulum cranes where their mathematical model is close to reality. In many cases, the crane system will exhibit a secondary swing characteristic that the load will swing around the hook since, for example, the mass of the hook cannot be ignored. Therefore, the existing control methods for single-pendulum cranes may not perform well when directly applied to the double-pendulum overhead crane system. As same as other control objects, in general, there are two main control directions: closed-loop control and open-loop control. With closed-loop control approaches, various control strategies have been applied to double pendulum cranes from linear based controls, such as tuned PID [1], decoupling linear with S curve trajectory [2], nonlinear quasi-PID [3], coupling PD with sliding mode control [4], to nonlinear controls [5], sliding mode control [6], Fuzzy control [7], optimal control [8], adaptive control [9], input-output inversion [10], etc. It is known that the closed-loop controllers require several sensors for measuring the hook and payload oscillation angles. These make it difficult for the closed-loop controls to be implemented in practice.

In opposition to closed-loop control, open-loop or feedforward control has been widely applied for vibration suppression control of double pendulum cranes. Multi-mode input preshaping technique has been effectively used for vibration suppression control of double pendulum cranes [11, 12, 13]. In addition, waveform command shaper [14, 15], smoother [16, 17, 18], and reference command shaping [19] have been applied to control double pendulum cranes. The open-loop control approaches use the know vibration information, such as vibration frequency and damping factor,

Received: 22 February 2022; Accepted: 23 May 2022.

to design the input filter to suppress the unwanted vibration. These methods are simple but effective in suppressing the payload vibration and can be implemented easily since they do not require vibration sensors.

The above feedforward control approaches are often combined with a closed-loop position controller for crane trolleys. Most of the cart position control is PID controller because of its simplicity, effectiveness, and applicability in practice. However, the stability and the performance of PID control may degrade when the system encounters interference from the environment or parameter uncertainties.

To further improve the system's performance while keeping the simplicity of the feedforward control system for crane control, in this paper, the Active Disturbance Rejection Control (ADRC) [20] is applied to control the trolley position instead of using PID control. With powerful disturbance rejecting ability and simplicity in design, ADRC is expected to replace traditional PID controller. Furthermore, the multi-mode input shaping (IS) is considered as a feedforward controller. Difference from other research that uses conventional input shapers such as Zero Vibration (ZV) and Zero Vibration Derivative (ZVD) shapers [21], this paper applies the Equal Shaping-Time and Magnitude (ETMn) shaper method [22], which is more robust than the traditional IS method without increasing the shaping time.

The rest of the paper is organized as follows. The mathematical model of the double pendulum crane is presented in section 2. In section 3, the design of ADRC control for the trolley is shown. In section 4, the traditional and ETMn input shaping is described. The combination of ADRC and the input shapers are presented in section 5. Conclusion and further studies are described in section 6.

2. Double Pendulum Crane Model

The double-pendulum crane system is illustrated in Figure 1, where x is the horizontal position of the trolley, m is the trolley mass, m_1 is the hook mass, m_2 is the payload mass, l_1 is the cable length between trolley and hook, l_2 is the cable length between hook and payload, θ_1 is the 1st sway angle and θ_2 is the 2nd sway angle. In this paper, for simplicity, all of the trolley, hook, and payload are considered as point masses, and the friction force between the trolley and the rail is neglected. The dynamic model of the double pendulum crane is described by (1), (2), and (3) [23, 28].

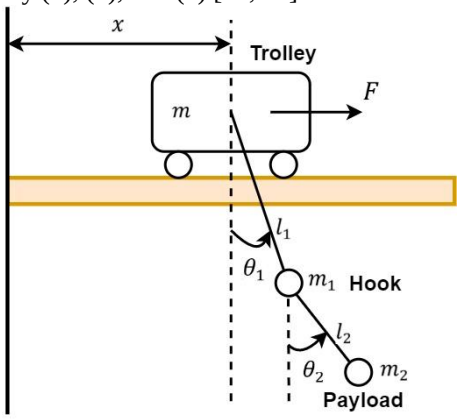

Figure 1: Schematic of two-dimensional double-pendulum crane [23]

$$\begin{cases} (m+m_1+m_2)\ddot{x} + (m_1+m_2)l_1(cos\theta_1\ddot{\theta}_1 - \dot{\theta}_1{}^2 sin\theta_1) + m_2 l_2(cos\theta_2\ddot{\theta}_2 - sin\theta_2\dot{\theta}_2{}^2) = F & (1) \\ (m_1+m_2)l_1 cos\theta_1\ddot{x} + (m_1+m_2)l_1{}^2\ddot{\theta}_1 + m_2 l_1 l_2[\cos(\theta_1-\theta_2)\,\ddot{\theta}_2 + \sin(\theta_1-\theta_2)\dot{\theta}_2{}^2] + (m_1+m_2)gl_1 sin\theta_1 = 0 & (2) \\ cos\theta_2\ddot{x} + l_1\cos(\theta_1-\theta_2)\,\ddot{\theta}_1 + l_2\ddot{\theta}_2 - l_1 sin(\theta_1-\theta_2)\dot{\theta}_1{}^2 + gsin\theta_2 = 0 & (3) \end{cases}$$

Assuming that the cable lengths do not change during the motion, the linearized equations of motion for this system (around a stable equilibrium point $\theta_1 = \theta_2 = 0$ are as follows [21]:

$$\ddot{\theta}_1(t) = -\left(\frac{g}{l_1}\right)\theta_1 + \left(\frac{gR}{l_1}\right)\theta_2 - \frac{u(t)}{l_1}$$
$$\ddot{\theta}_2(t) = \left(\frac{g}{l_1}\right)\theta_1 - \left(\frac{g}{l_2} + \frac{gR}{l_2} + \frac{gR}{l_1}\right)\theta_2 - \frac{u(t)}{l_1} \quad (4)$$

where $R = \frac{m_2}{m_1}$ is the ratio of the payload mass to the hook mass, g is the gravitational acceleration, and $u(t)$ is the acceleration of the trolley.

The two linearized frequencies of the double-pendulum are [23]:

$$\omega_1 = \sqrt{\frac{g}{2}(\alpha - \sqrt{\beta})} \quad (5)$$

$$\omega_2 = \sqrt{\frac{g}{2}(\alpha + \sqrt{\beta})} \quad (6)$$

where

$$\alpha = \frac{m_1+m_2}{m_1}\left(\frac{1}{l_1}+\frac{1}{l_2}\right)$$
$$\beta = \left(\frac{m_1+m_2}{m_1}\right)^2\left(\frac{1}{l_1}+\frac{1}{l_2}\right)^2 - 4\left(\frac{m_1+m_2}{m_1}\right)\frac{1}{l_1 l_2}$$

The payload vibration of a double pendulum crane is the combination of two single-frequency vibrations. Thus, to suppress the payload vibration using the feedforward control approach, multi-mode input shaping is considered in this paper. In addition, we will apply the ADRC controller for the trolley position controller instead of PID controller. The complete control system for the double pendulum crane is a combination of ADRC and multi-mode input shaping.

3. Control System Design

3.1. Position control of the trolley

3.1.1. *ADRC concept*

The concept of ADRC was initially proposed by J.Han [20]. In this paper, the work is focused on the second-order ADRC as follows:

$$\ddot{y}(t) = f(t) + b_0.u(t) \quad (7)$$

where u is the control signal, y is the output response, and f is a generalized disturbance (including input disturbance and parameter uncertainty). According to Han, the generalized term f is insignificant, while only its real-time estimates $\hat{f}$ is important. Therefore, an Extended State Observer (ESO) is designed to estimate $\hat{f}$ such that we can compensate the

impact of the disturbance to the process. So, we design the control law as:

$$u = (u_0 - \hat{f})/b_0 \quad (8)$$

to reduce the equation (4) to a form of:

$$\ddot{y}(t) \approx u_0 \quad (9)$$

which can be easily controlled. As stated above, ADRC requires little knowledge of the plant; all we need to know is the order of the plant and the value of the parameter b_0.

The ESO became more practical since a tuning method was proposed by Gao [24, 25]. The main idea is to use an augmented state-space model of equation (7) that includes f as an additional state. In particular, let:

$$x_1 = y,\ x_2 = \dot{y},\ x_3 = f \quad (10)$$

Then the ESO can be designed as:

$$\begin{cases} \dot{\hat{x}}_1(t) = \hat{x}_2(t) + l_1(y(t) - \hat{x}_1(t)) \\ \dot{\hat{x}}_2(t) = \hat{x}_3(t) + b_0.u(t) + l_2(y(t) - \hat{x}_1(t)) \\ \dot{\hat{x}}_3(t) = l_3(y(t) - \hat{x}_1(t)) \end{cases} \quad (11)$$

where l_1, l_2, l_3 are observer parameters, $\hat{x}_1$, $\hat{x}_2$, $\hat{x}_3$ are estimated values of y, $\dot{y}$, f respectively.

The control law in second-order ADRC is:

$$u = (u_0 - \hat{x}_3)/b_0 \quad (12)$$

$$u_0 = K_P(r - \hat{x}_1) - K_D.\hat{x}_2 \quad (13)$$

With $\hat{x}_3 \approx f$ obtained from ESO, (12) reduces (7) to an approximate double integral plant (9). Then, substituting (13-10) to (9) yields the closed-loop dynamic characteristic:

$$\ddot{y}(t) \approx u_0 = K_P\big(r(t) - y(t)\big) - K_D.\dot{y}(t) \quad (14)$$

where r is the setpoint, K_P and K_D are controller parameters. Taking the Laplace Transform of (14-11), one has the close-loop transfer function as follows:

$$G_{cl}(s) = Y(s)/R(s) = K_P/(s^2 + K_D.s + K_P) \quad (15)$$

So K_P and K_D can be easily calculated for the process to be controlled.

The structure of second-order ADRC is illustrated in Figure 2

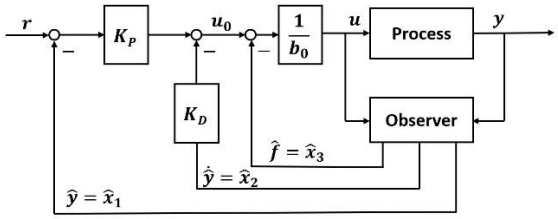

Figure 2: Second order ADRC control scheme

3.1.2. *Using ADRC to control trolley position*

To apply the ADRC presented in previous section, rewriting (1) to the same form as (4):

$$\ddot{x} = -[(m_1 + m_2)l_1(cos\theta_1\ddot{\theta}_1 - \dot{\theta}_1{}^2 sin\theta_1) + m_2 l_2 cos\theta_2\ddot{\theta}_2 - m_2 l_2 sin\theta_2\dot{\theta}_2{}^2]/(m + m_1 + m_2) + [1/(m + m_1 + m_2)]F = f(t) + b_0.u(t) \quad (16)$$

where

- $f(t) = -[(m_1 + m_2)l_1(cos\theta_1\ddot{\theta}_1 - \dot{\theta}_1{}^2 sin\theta_1) + m_2 l_2 cos\theta_2\ddot{\theta}_2 - m_2 l_2 sin\theta_2\dot{\theta}_2{}^2]/(m + m_1 + m_2)$
- $u(t) = F$
- $b_0 = \frac{1}{(m+m_1+m_2)}$

According to [26], the ADRC's parameters can be obtained as follow:

- Get the desired 2% settling time T_{settle}.
- Choose K_P and K_D to get a negative-real double pole, $s_{\frac{1}{2}}^{CL} = s^{CL}$:

$$K_P = (s^{CL})^2,\ K_D = -2.s^{CL} \quad (17)$$

with $s^{CL} = -\frac{6}{T_{settle}}$.

- Since the observer dynamics must be fast enough, the observer poles $s_{\frac{1}{2}}^{ESO}$ must be placed left of the closed-loop s^{CL}, for suggestion:

$$s_{\frac{1}{2}}^{ESO} = s^{ESO} \approx (3 \dots 10).s^{CL} \quad (18)$$

- The observer parameters can be chosen as:

$$l_1 = -3.s^{ESO},\ l_2 = 3.(s^{ESO})^2,\ l_3 = (s^{ESO})^3 \quad (19)$$

3.2. Vibration Suppression

3.2.1. *Input Shaping concept*

The traditional input shaping [27] can be summarized as follow. Let's consider the second-order vibratory system with the transfer function as

$$\frac{Y(s)}{U(s)} = \frac{\omega_n^2}{s^2 + 2\zeta\omega_n + \omega_n^2} \quad (20)$$

where ω_n is the undamped natural frequency and ζ is the damping ratio. If we apply an impulse $u_i(t) = A_i\delta(t - t_i)$ at time t_i with magnitude A_i, then the output of the vibratory system is

$$y_i(t) = A_i \frac{\omega_n}{\sqrt{1-\zeta^2}} e^{-\zeta\omega_n(t-t_i)} \sin\left(\omega_n\sqrt{1-\zeta^2}(t - t_i)\right) \quad (21)$$

When an impulse is applied, the system vibrates, as shown in (21). The idea of the input shaping method is to apply a series of impulses with appropriate magnitude in the proper time to the system. Then, those impulse responses eliminate each other, and the vibration is suppressed. The value of magnitude A_i and time t_i can be determined by setting the combination response equal to zero when the last impulse is applied. In the case of two impulse series called Zero Variation (ZV), the result is as follows:

$$\begin{cases} A_1 = \frac{1}{1+K},\ t_1 = 0 \\ A_2 = \frac{K}{1+K},\ t_2 = \frac{\pi}{\omega_d} \end{cases} \quad (22)$$

where

$$K = \exp\left(-\frac{\pi\zeta}{\sqrt{1-\zeta^2}}\right),\ \omega_d = \omega_n\sqrt{1-\zeta^2} \quad (23)$$

To increase the robustness with the modeling error, zero vibration and derivative (ZVD) shaper with three impulses is proposed:

$$\begin{cases} A_1 = \frac{1}{1+2K+K^2},\ t_1 = 0 \\ A_2 = \frac{2K}{1+2K+K^2},\ t_2 = \frac{\pi}{\omega_d} \\ A_3 = \frac{K^2}{1+2K+K^2},\ t_3 = \frac{2\pi}{\omega_d} \end{cases} \quad (24)$$

And zero vibration derivative and derivative (ZVDD) shaper with four impulses:

$$\begin{cases} A_1 = \frac{1}{1+3K+3K^2+K^3},\ t_1 = 0 \\ A_2 = \frac{3K}{1+3K+3K^2+K^3},\ t_2 = \frac{\pi}{\omega_d} \\ A_3 = \frac{3K^2}{1+3K+3K^2+K^3},\ t_3 = \frac{2\pi}{\omega_d} \\ A_4 = \frac{K^3}{1+3K+3K^2+K^3},\ t_4 = \frac{3\pi}{\omega_d} \end{cases} \quad (25)$$

3.2.2. *Impulse Vector for Input Shaping control*

Another approach to dealing with the input shaping technique is an impulse vector [22]. The idea of the impulse vector approach is to present the impulse response of a vibratory system by a vector. The response (21) of the vibratory system with impulse input $u_i(t) = A_i\delta(t - t_i)$ can be presented as a vector in a 2D polar coordinate system with a magnitude I_i and angle θ_i as shown in Figure 3, with

$$I_i = A_i e^{\zeta\omega_n t_i},\ \theta_i = \omega_d t_i, \quad (26)$$

For a positive impulse ($A_i > 0$), the initial point of the impulse vector is located at the origin of the polar coordinate system, while for a negative impulse ($A_i < 0$), the terminal point of the impulse vector is located at the origin.

Using vector diagram approach, ZV and ZVD^n shapers can be redesigned [22]. For the ZV shaper, let the first impulse vector be located at 0 on an impulse vector diagram because the first impulse's time location is $t_1 = 0$. The second impulse vector must be located at π with the same magnitude. ZVD, ZVDD, and ZVDDD shapers can be presented in Figure 4. ZVD shapers have three impulse vectors in which the first impulse vector is located at 0, the second at π, and the third at 2π. The magnitude ratio of the ZVD shaper is $I_1 : I_2 : I_3 = 1 : 2 : 1$. ZVDD shaper has four impulse vectors in which the first impulse vector is located at 0, the second at π, the third at 2π, and the fourth at 3π. The magnitude ratio of the ZVDD shaper is $I_1 : I_2 : I_3 : I_4 = 1 : 3 : 3 : 1$.

3.2.3. *ETMn input shaper*

The ETMn input shaper arranges the same magnitude impulse vectors and angle inside a 2π circle time. The digit "n" in "ETMn" is a positive integer, representing the number of participating vectors. The amplitude and phase angle of the ETMn method are listed below [22]:

$$\theta_1 = 0, \theta_2 = \frac{2\pi}{n-1}, \dots, \theta_{n-1} = \frac{(n-2).2\pi}{n-1}, \theta_n = 2\pi \quad (27)$$

$$I_2 = I_3 = \cdots = I_{n-1} = I_1 + I_n,\ I_n = mI_1 (m > 0) \quad (28)$$

The advantage of this ETMn method is that no matter how many impulse vectors are present, these vectors all fit inside a 2π circle time, which is equivalent to the shaping time of the ZVD method.

The ETM4 shaper has four impulse vectors, as shown in Figure 5. The impulse instants t_1, t_2, t_3, t_4 of the ETM4 shaper are obtained by the angles of the impulse vectors in equation (27). The impulse magnitudes A_1, A_2, A_3, A_4 of the ETM4 shaper are obtained by solving:

$$\begin{cases} I_2 = I_3 = I_1 + I_4,\ I_4 = mI_1 \\ I_1 = A_1, I_2 = A_2 e^{\zeta\omega_n t_2}, I_3 = A_3 e^{\zeta\omega_n t_3}, I_4 = A_4 e^{\zeta\omega_n t_4} \\ A_1 + A_2 + A_3 + A_4 = 1 \end{cases} \quad (29)$$

The resulting ETM4 shaper is:

$$\begin{bmatrix} t_i \\ A_i \end{bmatrix} = \begin{bmatrix} 0 & \frac{2\pi}{3\omega_d} & \frac{4\pi}{3\omega_d} & \frac{2\pi}{\omega_d} \\ \frac{I}{1+m} & \frac{I}{K^{\frac{2}{3}}} & \frac{I}{K^{\frac{4}{3}}} & \frac{mI}{(1+m)K^2} \end{bmatrix} \quad (30)$$

where

$$I = \frac{(1+m)K^2}{K^2 + (1+m)\left(K^{\frac{2}{3}} + K^{\frac{4}{3}}\right) + m},\ K = e^{\frac{\zeta\pi}{\sqrt{1-\zeta^2}}}$$

Similarly, we get the result with ETM5:

$$\begin{bmatrix} t_i \\ A_i \end{bmatrix} = \begin{bmatrix} 0 & \frac{\pi}{2\omega_d} & \frac{\pi}{\omega_d} & \frac{3\pi}{2\omega_d} & \frac{2\pi}{\omega_d} \\ \frac{I}{1+m} & \frac{I}{K^{\frac{1}{2}}} & \frac{I}{K} & \frac{I}{K^{\frac{3}{2}}} & \frac{mI}{(1+m)K^2} \end{bmatrix} \quad (31)$$

where

$$I = \frac{(1+m)K^2}{K^2 + (1+m)\left(K^{\frac{1}{2}} + K + K^{\frac{3}{2}}\right) + m},\ K = e^{\frac{\zeta\pi}{\sqrt{1-\zeta^2}}}$$

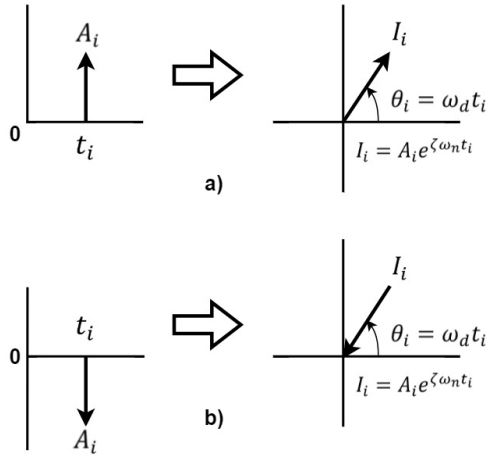

Figure 3: Impulse functions and their corresponding impulse vectors.
a) Positive impulse b) Negative impulse

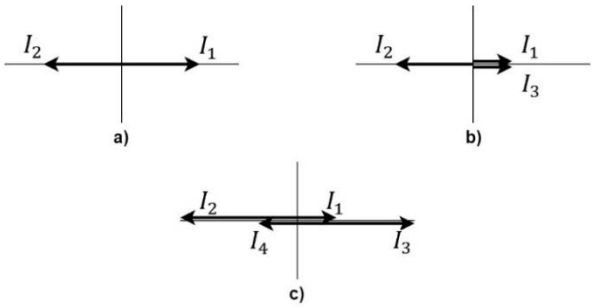

Figure 4: Impulse vector diagrams for the ZV and ZVD^n shapers

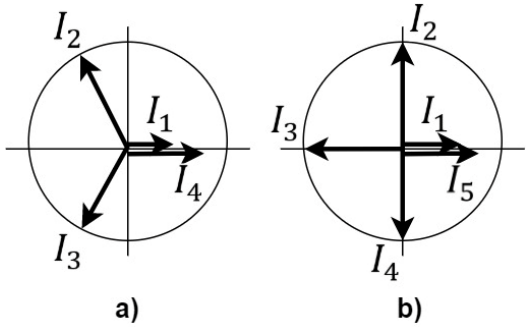

Figure 5: The impulse vector diagrams of the ETMn shapers.
a) ETM4 shaper b) ETM5 shaper

To obtain the optimal value of *m*, a performance index J is defined as the integral along the sensitivity curve with a sensitivity ratio $\frac{\omega_n}{\hat{\omega}_n}$ in a considered range, for example, 0.2 to 1.8.

$$J = \int_{r_l}^{r_u} V(r,m)dr,\ r = \frac{\omega_n}{\hat{\omega}_n}, m = \frac{I_n}{I_1}, r_l = 0.2, r_u = 1.8 \quad (32)$$

Table 1 represents optimal values m_{opt} for various ETMn shapers [22].

Table 1: The optimal values m_{opt} for various ETMn shapers

ζ	0	0.01	0.05	0.1	0.2	0.3	0.4	0.5
m_{opt}, ETM4	1	0.99	0.95	0.90	0.79	0.69	0.56	0.40
m_{opt}, ETM5	1	0.98	0.92	0.85	0.69	0.53	0.34	0.08

3.3. ADRC and Input shaping combination for double pendulum crane control

The control scheme is proposed in Figure 6, where ADRC is used to control the trolley position, and IS is used to suppress the vibration of the payload. Despite parameter uncertainty and disturbance, the ADRC guarantees to precisely control the trolley position. However, the ADRC control cannot suppress the payload vibration since it does not use vibration feedback. Thus, IS control is used as a filter to suppress the payload vibration. As mentioned in the previous section, the sway angles of the double-pendulum crane include two vibration frequencies, so to suppress the vibration of the payload, we need two shapers. The first shaper suppresses the first vibration, and the second shaper suppresses the second vibration. The final shaper is the convolution of two shapers corresponding to two vibration frequencies.

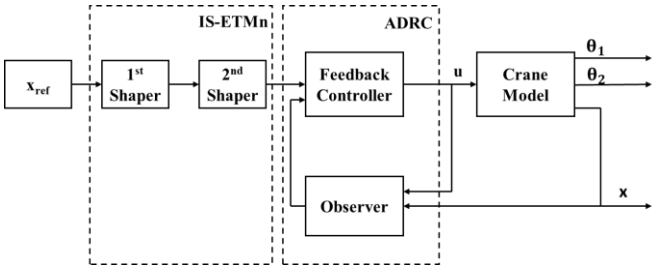

Figure 6: ADRC with IS controller

4. Validation via Simulation

To verify the effectiveness of the proposed control scheme, a simulation is conducted through Matlab/Simulink environment. Table 2 shows the system parameters [28].

Table 2: System parameters

m(kg)	20	m_2(kg)	5	l_2(m)	0.2	x_{ref}(m)	1.5
m_1(kg)	5	l_1(m)	2	g(m/s^2)	9.8	-	-

The parameters for ADRC controller design are chosen as $b_0 = 1/(m + m_1 + m_2) = 0.0333$, $T_{settle} = 8(s)$ and $s^{ESO} = 10s^{CL}$

The ZVD and ETM4 shaper parameters are given in Table 3 and 4 respectively.

Table 3: ZVD parameters

1st shaper		2nd shaper	
$A_1 = 0.25$	$t_1 = 0$	$A_1 = 0.25$	$t_1 = 0$
$A_2 = 0.5$	$t_2 = 1.456$	$A_2 = 0.5$	$t_2 = 0.309$
$A_3 = 0.25$	$t_3 = 2.912$	$A_3 = 0.25$	$t_3 = 0.618$

Table 4: ETM4 parameters

1st shaper		2nd shaper	
$A_1 = 1$	$t_1 = 0$	$A_1 = 0.1$	$t_1 = 0$
$A_2 = 2$	$t_2 = 0.97$	$A_2 = 0.2$	$t_2 = 0.20$
$A_3 = 2$	$t_3 = 1.94$	$A_3 = 0.2$	$t_3 = 0.412$
$A_4 = 1$	$t_4 = 2.912$	$A_4 = 0.1$	$t_4 = 0.618$

We will compare the performance of unshaped+ADRC controller with ZVD+ADRC controller and ETM4+ADRC controller.

In the first simulation, the trolley displacement and sway angle with three considered controllers are shown in Figure 7 and 8 respectively. For trolley displacement, all controllers have good performance. ZVD+ADRC and ETM4+ADRC has the same response. For payload sway angle, except unshaped+ADRC controller, other controllers suppress vibration fast. Figure 9 is control signal of these controllers.

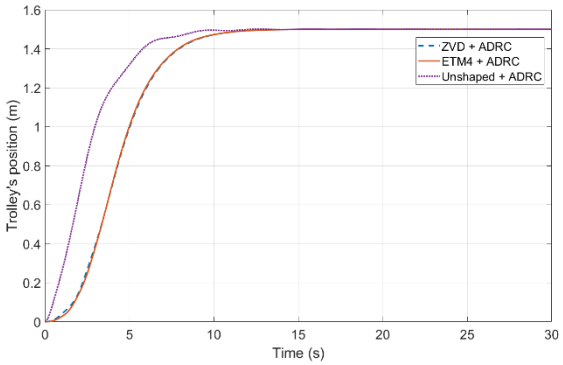

Figure 7: Trolley position

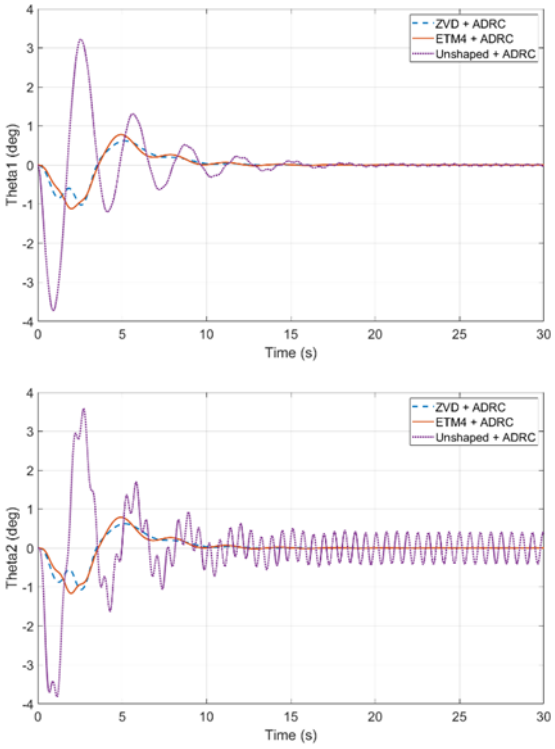

Figure 8: Crane sway angles

The next simulation will compare ZVD shaper and ETM4 shaper with payload mass variation from 5(kg) to 2(kg) and 20(kg) in Figure 10 to 15. All the controller parameters will be kept unchanged to examine the robustness of two

controllers. It can be seen that, with payload variation, ETM4 controller and ZVD controller show robustness in vibration suppression. Besides, when the payload change, the ETM4+ADRC controller suppress the vibration better than the ZVD+ADRC controller.

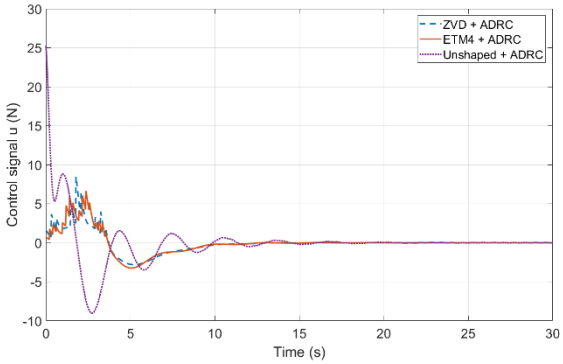

Figure 9: Control signal

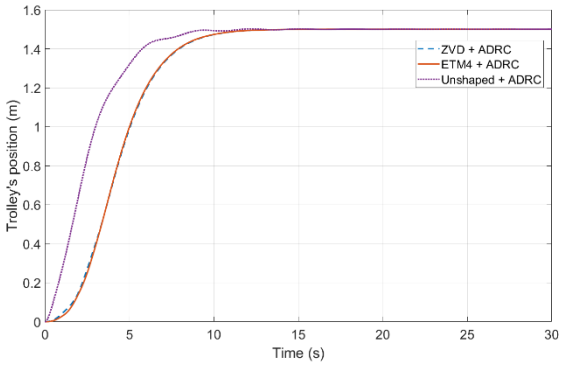

Figure 10: Trolley position when payload is 2(kg)

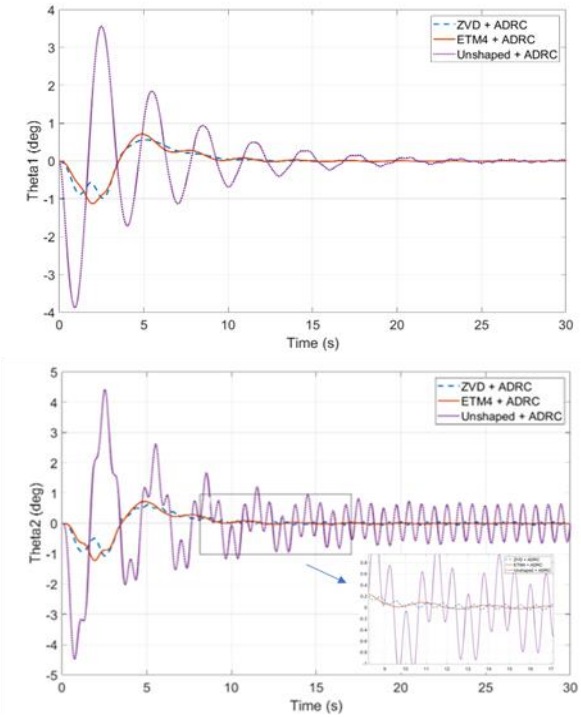

Figure 11: Crane sway angles when payload is 2(kg)

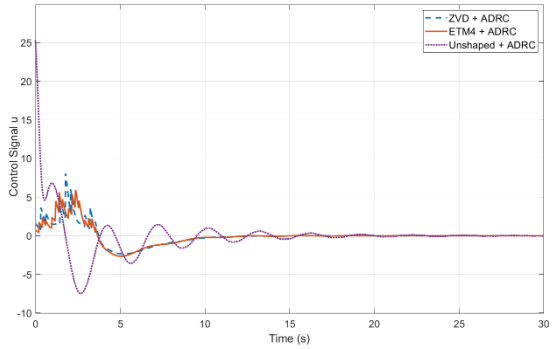

Figure 12: Control signal u when payload is 2(kg)

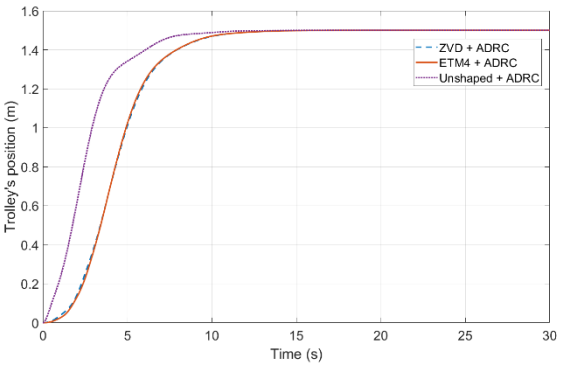

Figure 13: Trolley position when the payload is 20(kg)

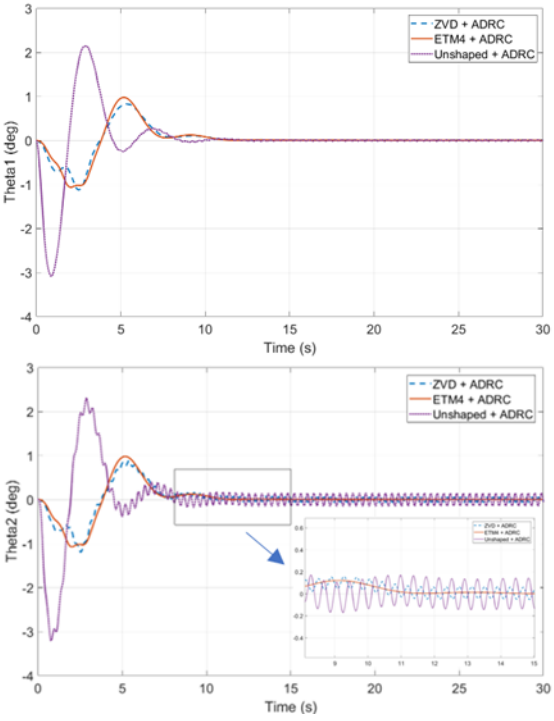

Figure 14: Crane sway angles when the payload is 20(kg)

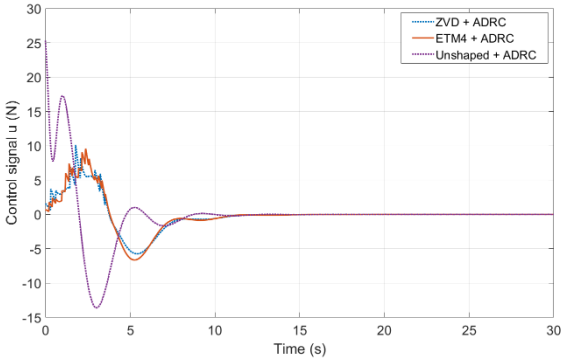

Figure 15: Control signal u when the payload is 20(kg)

5. Conclusion

The article has presented the combination of linear ADRC and IS-ETM4 input shaper for vibration suppression control of a double-pendulum crane system. The proposed controller has a simple design process while guaranteeing precise position control of the trolley and vibration suppression of the payload. The effectiveness of the proposed control algorithm has been validated by simulation. In the next step, the practical implementation of this approach will be done. The problem of reducing residual vibration caused by disturbance will be considered. In addition, its applications in other systems can also be considered.

Acknowledgment

This research is funded by Hanoi University of Science and Technology (HUST) under grant number T2021-PC-002.

References

[1] H.I. Jaafar, Z. Mohamed, N.A. Mohd Subha, A.R. Husain, F.S. Ismail, L. Ramli, M.O. Tokhi, M.A. Shamsudin (2019), *Efficient control of a nonlinear double-pendulum overhead crane with sensorless payload motion using an improved PSO-tuned PID controller*, J. Vib. Control., 25 (2019), pp. 907-921

[2] H. Ouyang, J. Hu, G. Zhang, L. Mei, X. Deng, *Decoupled linear model and S-shaped curve motion trajectory for load sway reduction control in overhead cranes with double-pendulum effect*, Proc. Inst. Mech. Eng. Part C J. Mech. Eng. Sci., 233 (2019), pp. 3678-3689

[3] N. Sun, T. Yang, Y. Fang, Y. Wu, H. Chen, *Transportation control of double-pendulum cranes with a nonlinear quasi-PID scheme: design and experiments*, IEEE Trans. Syst. Man Cybern. Syst., 49 (2019), pp. 1408-1418

[4] M. Zhang, Y. Zhang, X. Cheng, *An enhanced coupling PD with sliding mode control method for underactuated double-pendulum overhead crane systems*, Int. J. Control. Autom. Syst., 17 (2019), pp. 1579-1588

[5] N. Sun, Y. Wu, Y. Fang, H. Chen, *Nonlinear antiswing control for crane systems with double-pendulum swing effects and uncertain parameters: design and experiments*, IEEE Trans. Autom. Sci. Eng., 15 (2018), pp. 1413-1422.

[6] H. Ouyang, J. Hu, G. Zhang, L. Mei, X. Deng, *Sliding-mode-based trajectory tracking and load sway suppression control for double-pendulum overhead cranes*, IEEE Access, 7 (2019), pp. 4371-4379.

[7] D. Qian, S. Tong, S. Lee, *Fuzzy-logic-based control of payloads subjected to double-pendulum motion in overhead cranes*, Autom. Constr., 65 (2016), pp. 133-143.

[8] Q. Wu, X. Wang, L. Hua, M. Xia, *Dynamic analysis and time optimal anti-swing control of double pendulum bridge crane with distributed mass beams*, Mech. Syst. Signal Process., 144 (2020), Article 106968.

[9] B. Lu, Y. Fang, N. Sun, *Enhanced-coupling adaptive control for double-pendulum overhead cranes with payload hoisting and lowering*, Automatica, 101 (2019), pp. 241-251.

[10] M. Giacomelli, F. Padula, L. Simoni, A. Visioli, *Simplified input-output inversion control of a double pendulum overhead crane for residual oscillations reduction*, Mechatronics, 56 (2018), pp. 37-47.

[11] [M. Kenison, W. Singhose, *Input shaper design for double-pendulum planar gantry cranes*, Proc. IEEE Int. Conf. Control Appl., Hawaii, USA (1999), pp. 539-544.

[12] W. Singhose, J. Lawrence, K. Sorensen, D. Kim, *Applications and educational uses of crane oscillation control*, FME Trans., 34 (2006), pp. 175-183.

[13] K.C.C. Peng, W. Singhose, S.S. Gurleyuk, *Initial investigations of hand-motion crane control with double-pendulum payloads*, Am. Control Conf., Montréal, Canada (2012), pp. 6270-6275.

[14] K.A. Alhazza, Z.N. Masoud, *Waveform command shaping control of multimode systems*, J. Sound Vib., 363 (2016), pp. 126-140.

[15] Z.N. Masoud, K.A. Alhazza, *A smooth multimode waveform command shaping control with selectable command length*, J. Sound Vib., 397 (2017), pp. 1-16.

[16] X. Xie, J. Huang, Z. Liang, *Vibration reduction for flexible systems by command smoothing*, Mech. Syst. Signal Process., 29 (2013), pp. 461-470

[17] J. Huang, X. Xie, Z. Liang, *Control of bridge cranes with distributed-mass payload dynamics*, IEEE/ASME Trans. Mechatronics, 20 (2015), pp. 481-486.

[18] R. Tang, J. Huang, *Control of bridge cranes with distributed-mass payloads under windy conditions*, Mech. Syst. Signal Process., 72–73 (2016), pp. 409-419.

[19] H.I. Jaafar, Z. Mohamed, M.A. Ahmad, N.A. Wahab, L. Ramli, M.H. Shaheed (2021), *Control of an underactuated double-pendulum overhead crane using improved model reference command shaping: Design, simulation and experiment*, Mechanical Systems and Signal Processing, Volume 151, 2021, https://doi.org/10.1016/j.ymssp.2020.107358.

[20] J. Han (2009) *From PID to Active Disturbance Rejection Control*, IEEE Transactions on Industrial Electronics, vol 56, issue 3, pp. 900-906, doi:10.1109/TIE.2008.2011621.

[21] Singhose, W., Kim, D., and Kenison, M. (2008). *Input Shaping Control of Double-Pendulum Bridge Crane Oscillations.* ASME. J. Dyn. Sys., Meas., Control. May 2008; 130(3): 034504. https://doi.org/10.1115/1.2907363

[22] C. G. Kang (2019) *Impulse Vectors for Input-Shaping Control: A Mathematical Tool to Design and Analyze Input Shapers*, IEEE Control Systems Magazine, vol 39, issue 4, pp 40-55, doi:10.1109/MCS.2019.2913610.

[23] Dianwei Qian (2018) *Anti-Sway Control For Cranes: Design and Implementation Using Matlab*, De Gruyter.

[24] Z. Gao, Y. Huang, J. Han (2001) *An Alternative Paradigm for Control System Design*, Proceedings of 40th IEEE Conference on Decision and Control, Orlando, Florida.

[25] Z. Gao (2003) *Scaling and Parameterization Based Controller Tuning*, Proceedings of the 2003 American Control Conference.

[26] G. Herbs (2013) *A Simulative Study on Active Disturbance Rejection Control as a Control Tool for Practitioners*, Electronics, vol 2, no.3, pp. 246-279, https://doi.org/10.3390/electronics2030246.

[27] Neil C. Singer, Warren P. Seering (1990) *Preshaping Command Inputs to Reduce System Vibration*, Journal of Dynamics System, Mesurement and Control, vol 112, no. 1, pp. 76-82, https://doi.org/10.1115/1.2894142.

[28] Lin Chai, Qihang Guo, Huikang Liu and Mingbo Ding (2021) *Linear Active Disturbance Rejection Control for Double-Pendulum Overhead Crane*, IEEE Access, vol 9, pp 52225-52237, doi:10.1109/ACCESS.2021.3070048.